Comparison of different methods of analysis of satellite geomagnetic anomalies over Italy

Bejo Duka
Department of Physics, Faculty of Natural Sciences, University of Tirana, Albania

Abstract
Different methods of analysis have been applied to satellite geomagnetic data that are claimed to be representative of the crustal geomagnetic field of the Italian area. The methods are compared with each other concluding that the SCHA is the best one. The downward continuation of the field by different methods gives different results, the most realistic are those of SCHA and RHA methods. Some remarks about each method and their results for the Italian area are presented.

Key words *regional magnetic analysis – geomagnetic anomalies – satellite data analysis*

1. Introduction

There are several methods of analysis of geomagnetic anomalies derived from satellite data over a restricted area. In order to compare the results of different methods for the Italian area we applied the following methods:

1) The Equivalent Source Inversion (ESI) using dipoles (Mayhew, 1979; Purucker, 1990) or monopoles (O'Brien and Parker, 1994).

2) The Rectangular Harmonic Analysis (RHA) (Nakagawa and Yukutake, 1985).

3) The Spherical Cap Harmonic Analysis (De Santis *et al.*, 1990; Haines, 1990).

For a certain data density, the smaller the study area the less accurate the results of any method are. In each method used we tried many cases of different source distribution and of different order of double Fourier series, in order to obtain the best accuracy of results under the restriction of the small area. On the other hand, in order to compare the results of different methods in the same conditions, we attempted to have roughly the same number of calculated coefficients by the inversion of field data.

2. Data distribution

The data, supplied by Istituto Nazionale di Geofisica represent the residual data of ΔF (total field anomalies) and ΔX, ΔY, ΔZ, (component anomalies), when the IGRF (up to degree $n_{max} = 10$) of epoch 1980 was subtracted from the original data acquired by MAGSAT. During this subtraction the contribution of spherical harmonics up to $n_{max} = 10$ of the core field and crustal field is cancelled (Haines, 1990). As the contribution of higher spherical harmonics of the core field to the observed geomagnetic field is negligible, we considered such a residual magnetic field as the field of crustal origin.

The data points used for the analyses are shown in fig. 1, the total number of data points

Mailing address: Dr. Bejo Duka, Department of Physics, Faculty of Natural Sciences, University of Tirana, Tirana, Albania; e-mail: bduka@fshn.tirana.al

being 4027. The area covered by data is bounded by meridians 2.5°E and 21.5°E and parallels 35°N and 49°N. The altitude of data points ranges in the interval 300-510 km and the altitude distribution are shown in fig. 2.

As it can be noted in fig. 1, the data distribution is not uniform over the region, there are places not covered by satellite paths and places with too dense data point concentration. We think that this nonuniformity is another reason, apart from the small area, for the worsening accuracy of the results. In order to obtain more uniform data we followed two ways: a) the averaging of data over altitude; and b) the interpolation of data. In the first way, for each field component we simply averaged all data inside every 0.5° latitude × 0.5° longitude bin (Haines, 1990), considering the averaged value as the field value in the altitude equal to the average of altitudes of data inside the bin. So, we get 907 data points uniformly distributed on latitude and longitude (as shown in fig. 3) but having different altitudes. In fig. 3, there are several «holes» in the bins where there are no original data points. Such average produces a significant deviation from the original field (the rms of deviation between the original field and averaged field was 1.01 nT for ΔF, 2.62 nT for ΔX, 2.39 nT for ΔY and 1.93 nT for ΔZ). However, the anomaly map does not un-

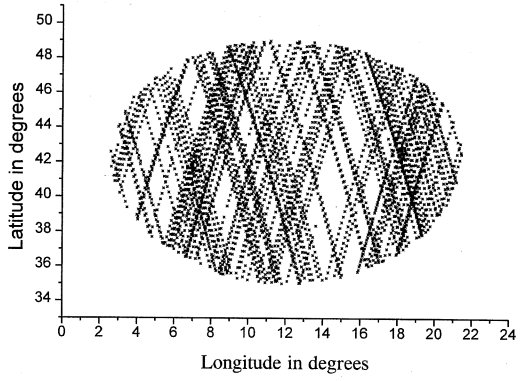

Fig. 1. Satellite data distribution over Italy.

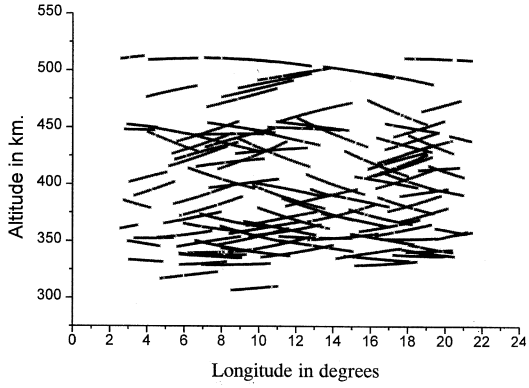

Fig. 2. Altitudes of satellite passes.

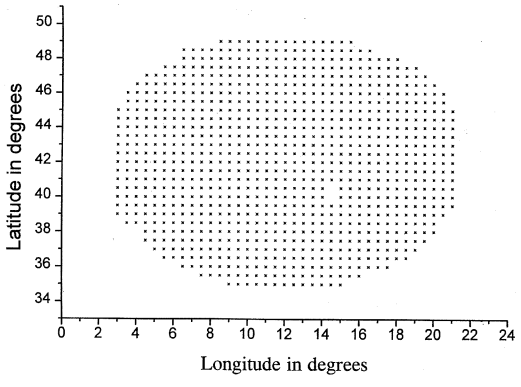

Fig. 3. Averaged satellite data distribution.

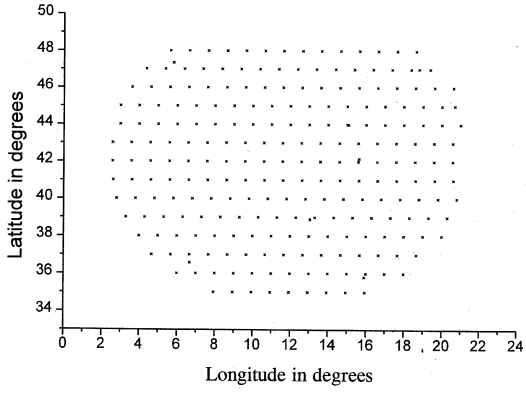

Fig. 4. Interpolated satellite data distribution.

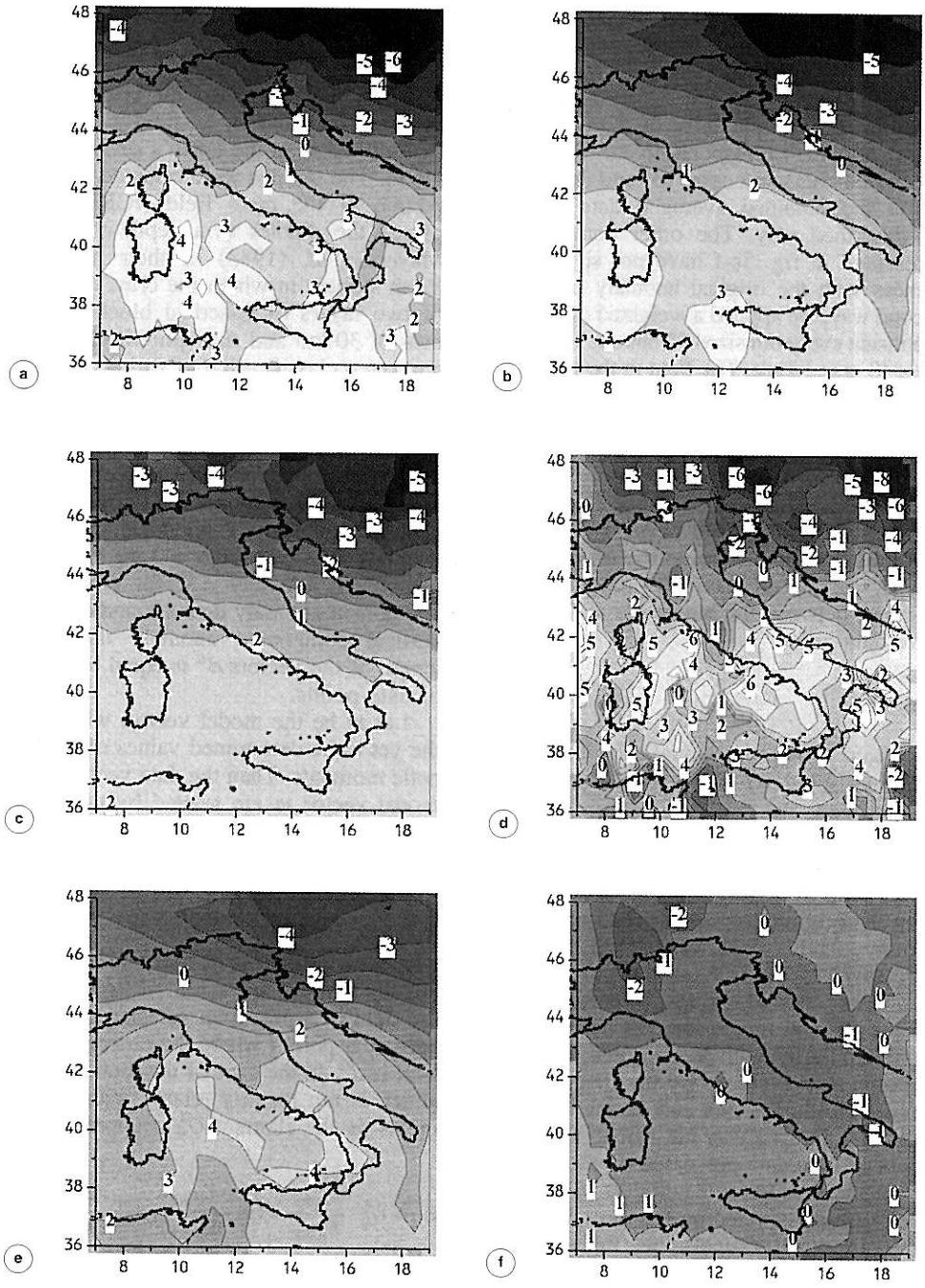

Fig. 5a-f. a) ΔF isolines of original data; b) ΔF isolines of averaged data; c) ΔF isolines of interpolated data; d) ΔZ isolines of original data; e) ΔZ isolines of averaged data; f) ΔZ isolines of interpolated data.

dergo great changes from the averaging, except some smoothing of the field with cancellation of some local small anomalies. Figure 5a-f shows the isolines of ΔF and ΔZ component of the data in the altitude interval 420-470 km, cases (a) and (d) correspond to the observed data (original data) and cases (b) and (e) correspond to the obtained averaged data by the above described way. The other components not presented in fig. 5a-f have not significant differences with the original anomaly maps. In the second way, we applied a weighted averaging of data inside every bin sized 1° latitude × 1° longitude × 40 km altitude. The field in the center of every bin is interpolated using the formula

$$F_i = \sum_j a_{ij} F_j$$

where F_i is the value of the field (ΔF, ΔX, ΔY, ΔZ) in the center of the ith bin and F_j are the field values data points inside the ith bin. The weights a_{ij} are chosen inversely proportional to the distance between the bin center and the respective data point

$$a_{ij} = \frac{c}{r_{ij}}.$$

The constant c of proportionality is found by the relation $\sum_j a_{ij} = 1$. If there is only one data point inside the bin, then this point is included in the data point grid (shown in fig. 4) without doing the interpolation for the bin center. After such averaging the rms of deviation between the original (observed) field and averaged (interpolated) field was 1.1 nT for ΔF, 2.61 nT for ΔX, 2.41 nT for ΔY and 1.98 nT for ΔZ. The anomaly maps (represented in fig. 5c for ΔF and fig. 5f for ΔZ) have almost the same similarity with the original anomaly maps as the data averaged by the first way. In the following illustrations and tables the data processed by the first way are named the averaged data and the data processed by the second way are named the interpolated data. All methods used here are applied on the three kinds of data: the observed (original) data, the averaged data and the interpolated data. In order to compare the results of different methods graphically we will present only the original data and averaged data.

3. Dipolar Equivalent Source Inversion (DESI)

In the DESI method the crustal anomalies are approximated by a field of an array of dipoles placed at the Earth's surface (Mayhew, 1979). The dipoles were oriented along the direction of the main field (IGRF). We have placed the dipoles at a depth of 15 km like Meyer *et al.* (1983) in their model of the Earth's crust, in which the crust is constructed of two layers of spherical blocks with thickness of 30 km and susceptibility selected from a ten step classification of various crustal types and the effect of each block has been approximated by a single dipole placed in the middle of the block.

The data are stored in the vectors $\boldsymbol{d}^\alpha$, where $\alpha = 1, 2, 3, 4$ represents the observed component *i.e.* for $\alpha = 1$ we have the total field anomaly data ΔF, for $\alpha = 2$ we have the north component anomaly ΔX, for $\alpha = 3$ the east component anomaly data ΔY and for $\alpha = 4$ the vertical component anomaly data ΔZ. The length of the vectors $\boldsymbol{d}^\alpha$ is equal to the number of data points.

Let $\boldsymbol{m}$ be the model vector, which contains the yet to be determined values of dipole magnetic moments. Then the data vector $\boldsymbol{d}^\alpha$ and the model vector $\boldsymbol{m}$ are related by the linear system of equations

$$d_i^\alpha = \sum_j G_{ij}^\alpha \cdot m_j \qquad (3.1)$$

where each element of the matrix G_{ij}^α contains the analytical expression of α-component of the field of a particular selected dipole m_j at a particular point i where the observed α component is d_i^α. In the case of the total field ($\alpha = 1$), which is not linearly related with dipolar moments m_j the element G_{ij}^1 is approximated as

$$G_{ij}^1 = G_{ij}^2 \cdot \frac{X_{\mathrm{IGRF}}}{F_{\mathrm{IGRF}}} + G_{ij}^3 \cdot \frac{Y_{\mathrm{IGRF}}}{F_{\mathrm{IGRF}}} + G_{ij}^4 \cdot \frac{Z_{\mathrm{IGRF}}}{F_{\mathrm{IGRF}}} \qquad (3.2)$$

i.e. each component of the dipole field is projected on to the direction of the main field (IGRF).

Table I. rms obtained by the Dipolar Equivalent Source Inversion (DESI).

Component	Original data		Averaged data		Interpolated data	
	20 dipoles rms (nT)	49 dipoles rms (nT)	20 dipoles rms (nT)	49 dipoles rms (nT)	20 dipoles rms (nT)	49 dipoles rms (nT)
ΔF	3.65	3.67	3.55	3.57	3.29	3.30
ΔX	3.41	3.37	2.25	2.19	2.14	2.08
ΔY	2.76	2.79	1.45	1.53	1.44	1.47
ΔZ	3.08	3.05	2.62	2.57	2.48	2.46

There is no exact solution to the eq. (3.1), but we are looking for the best approximated solution $\boldsymbol{m}'$, in the sense of minimizing the L_2 norm of prediction error:

$$\| G^{\alpha} \cdot \boldsymbol{m}' - \boldsymbol{d}^{\alpha} \|_2 = \min .$$

In our calculation of the model vector $\boldsymbol{m}'$, where the number of dipoles is less than the number of data (the overdetermined problem in eq. (3.3)) we have used the program ZAPP (Malin *et al.*, 1982). We have tried with different sets of dipoles in order to obtain the best fit between the observed data and the field calculated by eq. (3.1) (when instead of $\boldsymbol{m}$ we have $\boldsymbol{m}'$). We presented here two cases: a set of 20 dipoles placed in a grid of $3° \times 2.5°$ and a set of 49 dipoles placed in a grid of $1.5° \times 1.5°$. Table I shows the rms deviation between the input field and calculated field for two cases, when the input field is that of original data (two first columns) or averaged data (two second columns) or interpolated data (two third columns). In all cases the standard deviation of the dipole moments is one order smaller than the values of dipole moments.

In order to compare graphically the input field (interpolated data) and calculated field (in the case of the model with 49 dipoles) we have drawn the ΔX, ΔY, ΔZ isolines of the calculated field at altitude 350 km respectively in figs. 6b, 7b and 8b and ΔX, ΔY, ΔZ isolines of the input field (interpolated data) at altitude interval 325-375 km respectively in figs. 6a, 7a and 8a.

According to (3.1) we can calculate the field at any altitude. So we calculated the field at the Earth's surface, which is thought to be a downward continuation of the observed field. But the field values were so large that they were not the downward continuation of the observed field. The reason is that any model formed by dipoles is not valid for an altitude close to the dipoles emplacement.

4. The Polynomial Equivalent Source Inversion (PESI)

We made a small change to the classical ESI method, considering that the value of dipolar moment in formula (3.1) can be expressed as a polynomial of latitude θ and longitude ϕ

$$m(\theta, \phi) = \sum_{k=0}^{k_{\max}} \sum_{l=0}^{k} A_{k,l} \cdot \theta^k \cdot \phi^l \cdot F(\theta, \phi) \qquad (4.1)$$

where $F(\theta, \phi)$ is the main field at the point (θ, ϕ).

Substituting $\theta = \theta_j$ and $\phi = \phi_j$ into (4.1) and then (4.1) into (3.1), we obtained a linear system of equations where the unknowns are the $A_{k,l}$ coefficients. Then following the algorithm of classical ESI we calculated the $A_{k,l}$ coefficients by the ZAPP program. The time spent by the computer was 20 times greater than for the DESI method. We tried many cases of different values of $k_{\max}$ and different grid θ, ϕ in the studied area. In the best case, when the standard deviation of coefficients were one order smaller than the values of coefficients, the value of $k_{\max}$ was 4 and the number of grid

Table II. rms obtained by the Polynomial Equivalent Source Inversion (PESI).

Component	Original data	Averaged data	Interpolated data
	rms (nT)	rms (nT)	rms (nT)
ΔF	4.17	2.69	2.50
ΔX	4.13	2.26	2.09
ΔY	2.81	2.13	2.02
ΔZ	4.22	2.33	2.25

points, where the value of dipolar moment is considered known, was 399 (a grid of nearly $0.9° \times 0.9°$).

The rms deviations between the input field and the calculated field are presented in table II both for the original data, the averaged data and the interpolated data.

The isolines of calculated anomalies at the same points as the input (interpolated data) field are shown in fig. 6c (for ΔX), fig. 7c (for ΔY), fig. 8c (for ΔZ).

For the same reason as for the previous model of dipoles we could not do the downward continuation of the field.

5. The Monopolar Equivalent Source Inversion (MESI)

We did not apply a regularized geomagnetic field modelling using monopoles like O'Brien and Parker (1994), but a simple one as follows. The reasons were not only the complication of the regularized modelling, but firstly, we wanted to compare different methods of modelling in the same conditions and secondly the results of O'Brien and Parker (1994) applying the regularized modelling for the MAGSAT data were not more accurate (the data are fitted to an rms level of 3.62 nT; O'Brien and Parker, 1994) than the other methods.

In the source-free region we can model the scalar potential of the geomagnetic field $\Phi(\boldsymbol{r})$ as a linear combination of potential sources (O'Brien and Parker, 1994):

$$\Phi(\boldsymbol{r}) = \sum_{k=1}^{K} \alpha_k \cdot \phi_k(\boldsymbol{r}) \qquad (5.1)$$

where α_k are the source strengths.

Supposing that the sources are monopoles located at points $\boldsymbol{s}_k$ on a sphere with radius s, then:

$$\phi_k(\boldsymbol{r}) = \frac{1}{|\boldsymbol{r} - \boldsymbol{s}_k|}. \qquad (5.2)$$

The set of data $\{d_j\}$, $j = 1, 2 \ldots N$ ($N \geq K$) are measurements of the field strength $\boldsymbol{B}(\boldsymbol{r}_j)$ in directions given by the unit vectors $\{\boldsymbol{e}_j\}$ and obtained at the positions $\boldsymbol{r}_j$, *i.e.* $d_j \approx \boldsymbol{e}_j \cdot \boldsymbol{B}(\boldsymbol{r}_j)$. Using $\boldsymbol{B}(\boldsymbol{r}) = -\nabla\Phi$ and relations (5.1)-(5.2), the data are related to the source strengths as

$$d_j \approx -\sum_{k=1}^{K} \alpha_k [\boldsymbol{e}_j \cdot \nabla\phi_k(\boldsymbol{r}_j)] = \sum_{k=1}^{K} \alpha_k \cdot G_{j,k} \qquad (5.3)$$

or more compactly

$$\boldsymbol{d} \approx G \cdot \alpha \qquad (5.4)$$

where $\boldsymbol{d}$ is the column vector of the data, α is the column vector of the source strength and G is the $N \times K$ matrix of Green's function given by formulas of O'Brien and Parker (1994, Appendix C, p. 578) (after correcting some printing errors!).

By the ZAPP program we calculated the α_i ($i = 1, 2 \ldots K$) source strengths. The data were ΔX, ΔY, ΔZ components of anomaly field of MAGSAT over Italy. In order to obtain the best fit between the input field and calculated field we tried many cases of different distribution and depth of the monopole sources.

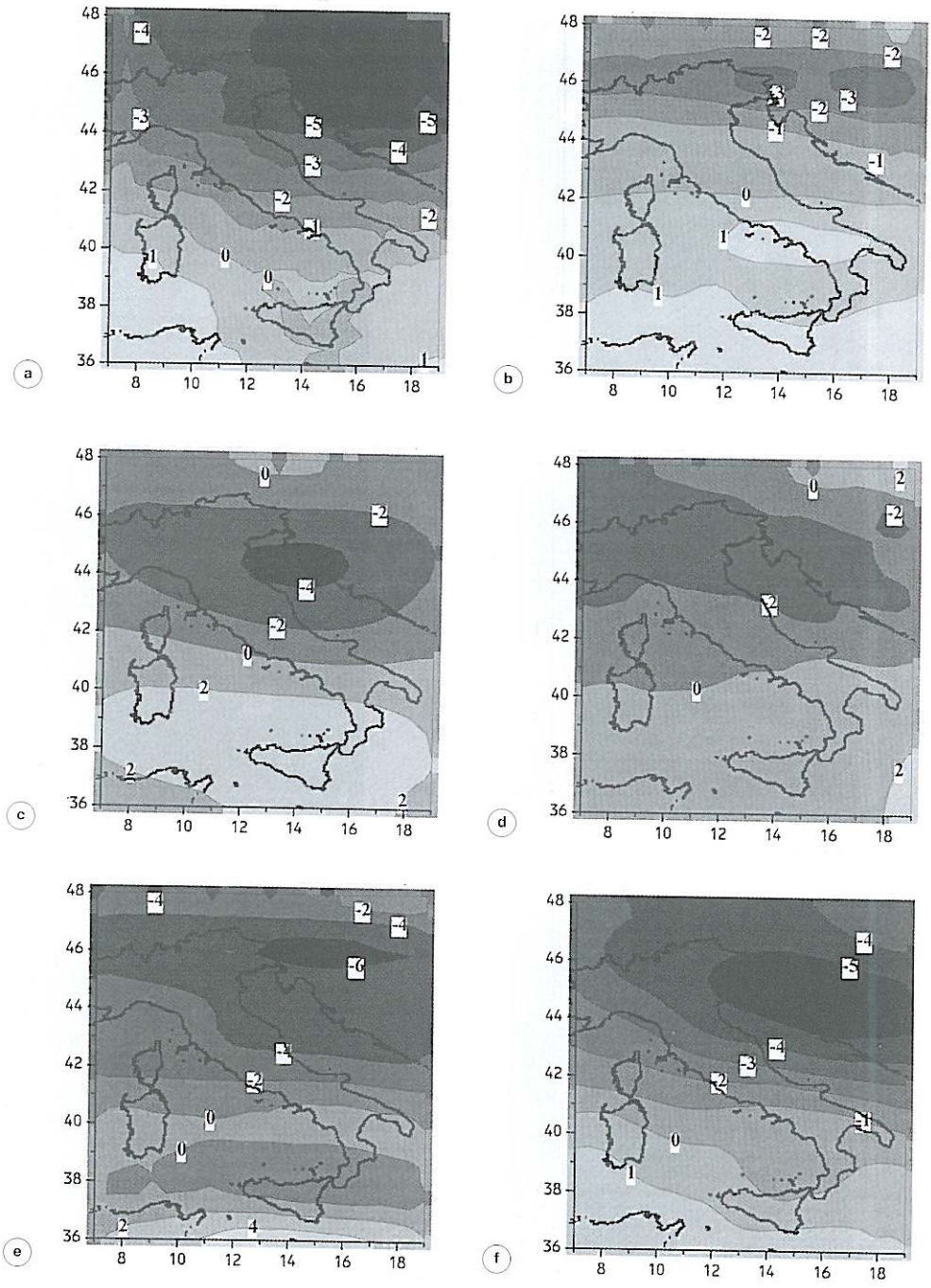

Fig. 6a-f. ΔX isolines of input field (a) and of calculated fields: DESI (b); PESI (c); MESI (d); RHA (e); SCHA (f).

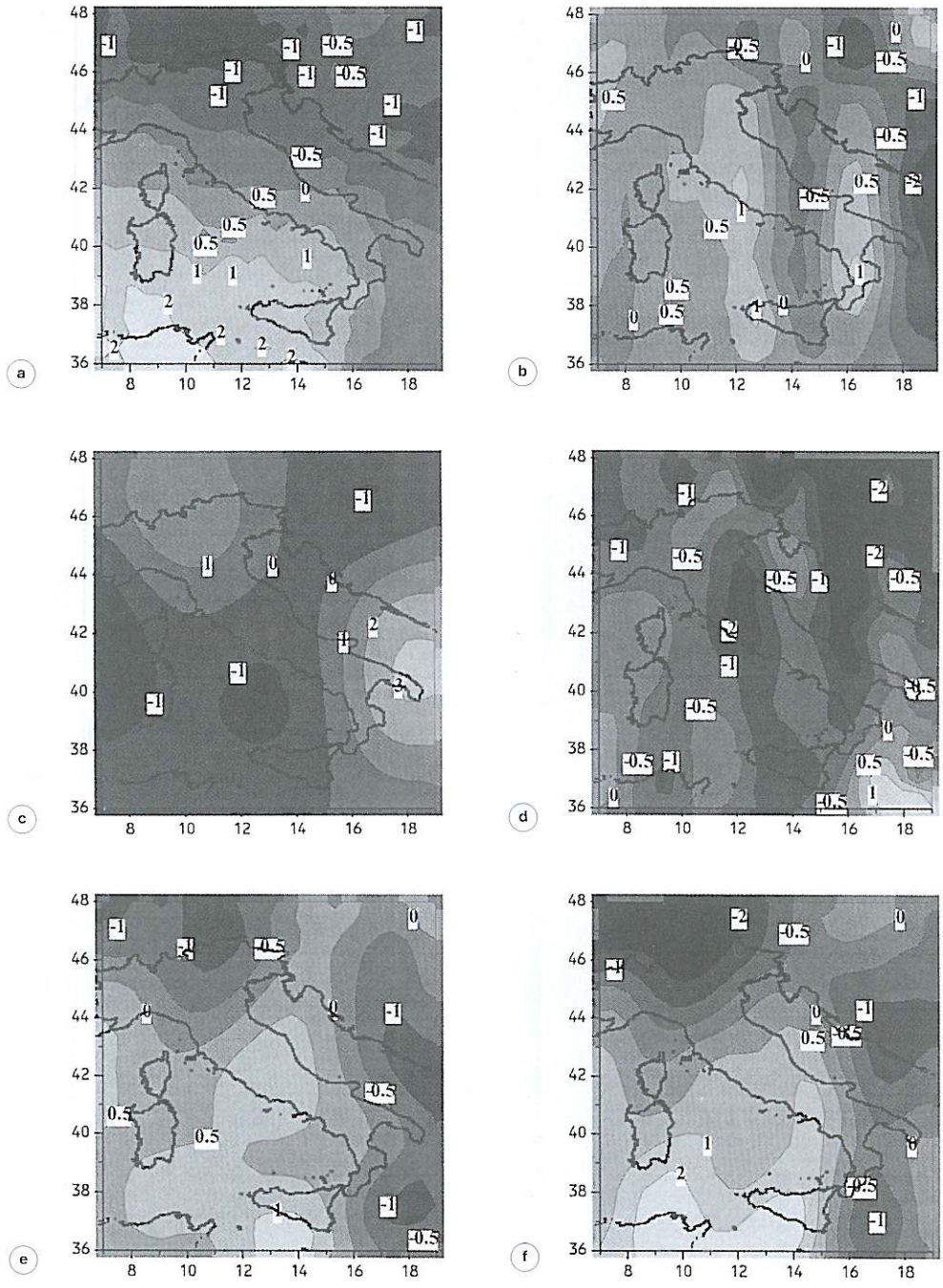

Fig. 7a-f. ΔY isolines of input field (a) and of calculated fields: DESI (b); PESI (c); MESI (d); RHA (e); SCHA (f).

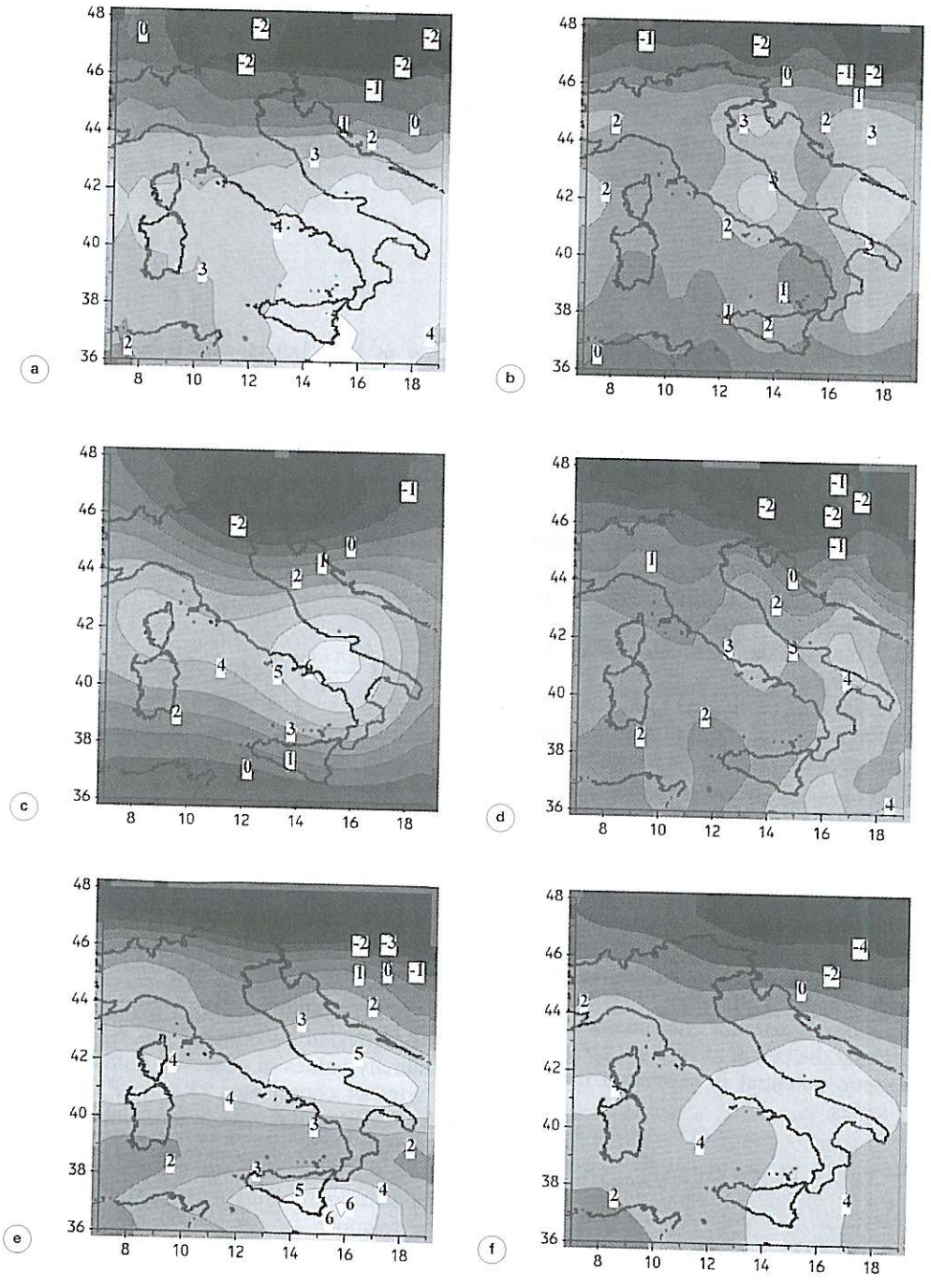

Fig. 8a-f. ΔZ isolines of input field (a) and of calculated fields: DESI (b); PESI (c); MESI (d); RHA (e); SCHA (f).

Table III. rms obtained by the Monopolar Equivalent Source Inversion (MESI).

Component	Original data		Averaged data		Interpolated data	
	16 monop. rms (nT)	100 monop. rms (nT)	16 monop. rms (nT)	100 monop. rms (nT)	16 monop. rms (nT)	100 monop. rms (nT)
ΔX	4.06	3.08	2.60	2.01	2.52	2.11
ΔY	3.55	2.76	1.72	1.68	1.61	1.59
ΔZ	2.13	2.07	2.21	1.53	2.08	1.70

In table III, we present the rms of fitting between the input field and output field for two sets of monopoles, one with 16 monopoles placed in a grid of $4.5° \times 3.5°$ at a depth of 80 km and another with 100 monopoles placed in a grid of $1.2° \times 1.2°$ at the same depth of 80 km.

For the same reasons as for the model of dipoles we could not do the downward continuation of the field, although the field of monopoles increases with the decreasing of distance from source more slowly than the field of dipoles.

The isolines of calculated field (for the set of 100 monopoles) at the altitude 350 km are shown in figs. 6d (for ΔX), 7d (for ΔY), 8d (for ΔZ).

6. The Rectangular Harmonic Analysis (RHA)

The RHA is applied to ΔX, ΔY, ΔZ data over the area of Italy following the way treated by Nakagawa and Yukutake (1985).

In the local Cartesian coordinates (x, y, z) with origin at the center of region (42°N, 12°E) the magnetic potential is expressed in double Fourier series

$$V = X_0 \cdot x + Y_0 \cdot y + Z_0 \cdot z + \sum_m \sum_n A_{m,n} \cdot \cdot \exp\left(\frac{2\pi imx}{L}\right) \cdot \exp\left(\frac{2\pi iny}{L}\right) \cdot \exp\left(\frac{2\pi lz}{L}\right) \quad (6.1)$$

where L is the length of the studied area and $l^2 = m^2 + n^2$. Introducing a normalization parameter N and the variables

$$u = \frac{N \cdot x}{L}, \quad v = \frac{N \cdot y}{L}, \quad w = \frac{N \cdot z}{L} \quad (6.2)$$

then the magnetic potential becomes

$$V' = X_0 u + Y_0 v + Z_0 w + \frac{N}{L} \cdot \sum_m \sum_n A_{m,n} \cdot \cdot \exp\left(\frac{2\pi imu}{N}\right) \cdot \exp\left(\frac{2\pi inv}{N}\right) \cdot \exp\left(\frac{2\pi lw}{N}\right). \quad (6.3)$$

Each component of the magnetic field is expressed

$$X = -\frac{\partial V'}{\partial u}, \quad Y = -\frac{\partial V'}{\partial v}, \quad Z = -\frac{\partial V'}{\partial w} \quad (6.4)$$

as a linear function of unknown coefficients X_0, Y_0, Z_0, $A_{m,n}$ ($A_{m,n}$ being a complex number).

After transforming the geocentric coordinates of satellite positions into normalized local Cartesian coordinates (u_i, v_i, w_i) and the anomaly values of observed field into the local Cartesian coordinates (X_i, Y_i, Z_i), we applied the ZAPP program in order to obtain the coefficients X_0, Y_0, Z_0, $A^{\text{real}}_{m,n}$, $A^{\text{complex}}_{m,n}$. To run the program well, we have to take only the independent coefficients as between them there is the relation:

$$A^{\text{real}}_{m,n} = A^{\text{real}}_{-m,-n}, \quad A^{\text{complex}}_{m,n} = -A^{\text{complex}}_{-m,-n}. \quad (6.5)$$

In order to avoid the edge effect, the data were

weighted to a 10 bell (Nakagawa and Yukutake, 1985).

Taking $N = 2$ and $L = 1600$ km for our area, we tried different maximum values of m,n. We noticed a deterioration of accuracy with increasing harmonics. In the best case the series were terminated at $n = 1$, $m = 1$. where the standard deviation is one order smaller than the values of coefficients. But in this case there are a small number of independent coefficients (only 11 of 21 coefficients). In order to compare the results with those taken from other methods we chose the maximum order $n = m = 3$. In this case we have 57 independent coefficients from 101 coefficients. Some coefficient values are in the same order as their standard deviation and the accuracy of fit between the input field and the output field deteriorated especially for the Z component (see table IV).

From X_0, Y_0, Z_0, $A_{m,n}$ coefficients defined by RHA (for $n = m = 3$) we can calculate the ΔX, ΔY, ΔZ at any altitude. Figure 9a-c shows the isolines of ΔX, ΔY, ΔZ respectively, calculated by RHA at the Earth's surface (altitude 0), that can be compared with the isolines of ΔX (fig. 6e), ΔY (fig. 7e), ΔZ (fig. 8e) calculated by RHA at the altitute 350 km.

7. The Spherical Cap Harmonic Analysis (SCHA)

We followed the modelling procedure described by De Santis *et al.* (1990) for the same data (these data are those we used in each method), for the same spherical cap with the center at 42°N, 12°E and the half-angle 7°, and the same number of coefficients ($k_{max} = 9$) giving a model of 100 coefficients in the expression of magnetic potential

$$V = a \sum_{k=0}^{k_{max}} \sum_{m=0}^{k} \left(\frac{a}{r}\right)^{n_k(m)+1} \cdot \cdot (g_k^m \cos(m\phi) + h_k^m \sin(m\phi)) \cdot P_{n_{k(m)}}^m (\cos\theta) \tag{7.1}$$

with noninteger harmonic degree $n_k(m)$ and Kmn Schmidt normalizing constants given in table I of De Santis *et al.* (1990, p. 1032).

By the inversion procedure we calculated the g_n^m and h_n^m coefficients, but we have to say that for some coefficients the standard deviation were in the same order as the values of coefficients. The rms of the fit between the input field (for the original and averaged data) and calculated field are presented in the table V.

Table IV. rms obtained by the Rectangular Harmonic Analysis (RHA).

Component	Original data	Averaged data	Interpolated data
	rms (nT)	rms (nT)	rms (nT)
ΔX	4.13	2.26	1.88
ΔY	2.81	2.13	1.32
ΔZ	4.22	2.33	1.81

Table V. rms obtained by the Spherical Cap Harmonic Analysis (SCHA).

Component	Original data	Averaged data	Interpolated data
	rms (nT)	rms (nT)	rms (nT)
ΔX	2.66	0.97	1.14
ΔY	2.45	0.86	1.02
ΔZ	1.82	0.65	0.87

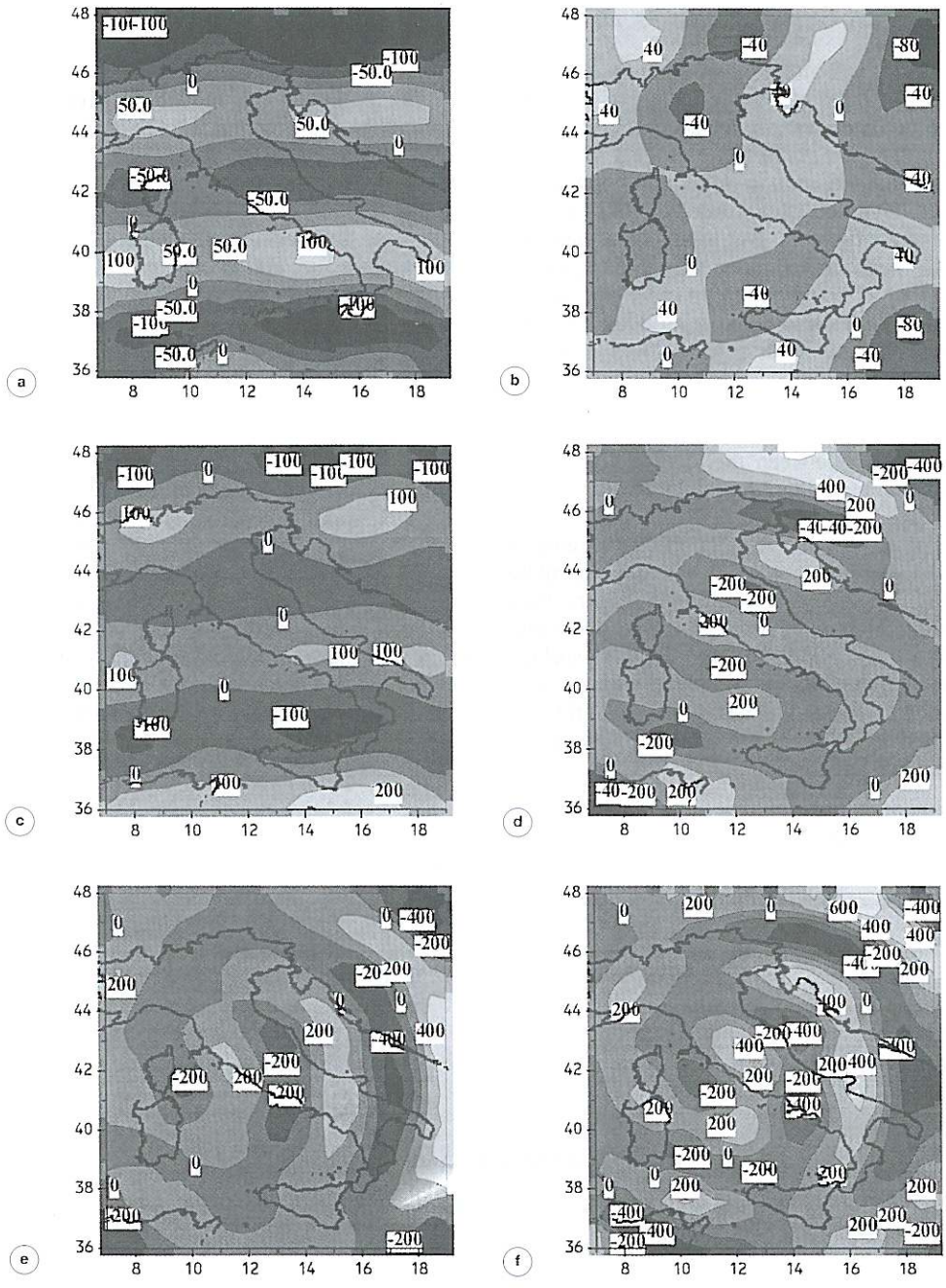

Fig. 9a-f. a) ΔX isolines at altitude 0 (RHA); b) ΔY isolines at altitude 0 (RHA); c) ΔZ isolines at altitude 0 (RHA); d) ΔX isolines at altitude 0 (SCHA); e) ΔY isolines at altitude 0 (SCHA); f) ΔZ isolines at altitude 0 (SCHA).

Figures 6f, 7f and 8f show the isolines of calculated field at the altitude 350 km and fig. 9d-f shows the isolines of the calculated field at the Earth's surface (altitude 0).

8. Discussion

Comparing figs. 6a-f, 7a-f and 8a-f we noticed that the calculated fields are similar to the observed field for all cases and all components. But the best similitude is for the total field and Z component anomalies and the best case is that of the SCHA method. Also numerically the best fit in each method is for the Z component and best fitting is for the SCHA method (the rms values are smaller than those from other methods). Almost all methods provide smooth fields with a tendency of isolines following the parallels for the X and Z components and following meridians for the Y component. Another common feature shared by all methods is that the calculated field has the strongest gradients on the edges of the chart. Presumably all methods are affected by edge effects.

We can find many models which fit well the data on the satellite altitude, but when we do the downward continuation of the field from the satellite height to the Earth's surface we find different results, in some cases unrealistic as in the cases of the DESI, PESI and MESI. In the case of PESI, the results depend too much on the order of polynomial (Malin *et al.*, 1982), and for the polynomial of order greater than 4 the running time of the computer program is extremely long.

The most realistic results of downward continuation of the anomalies are those of the RHA and SCHA methods. For the RHA method the attenuation of the harmonics with the increase in altitude depends on the wavelength so that for $n = -1,0, +1$; $m = -1,0, +1$ (wavelength greater than 1600 km) this attenuation is negligible, while for $n = 3$, $m = 3$ (wavelength nearly 500 km) the attenuation is about 100 fold. The picture of the field does not change much during the downward continuation except that some new anomalies with short wavelength appear.

Using the SCHA method for the downward continuation of the field, the values of the field are increased of about 100 fold and some local short wavelength anomalies appear. Some of those anomalies are due to the edge effect which is more evident in the SCHA method.

The interpretation of MAGSAT anomalies of Italy was not the subject of this work. There are two different works by Nolte and Hahn (1992) and Taylor and Ravat (1995) on the interpretation of MAGSAT anomalies of Central Europe.

REFERENCES

DE SANTIS, A., O. BATTELLI and D.J. KERRIDGE (1990): Spherical cap harmonic analysis applied to regional field modelling for Italy, *J. Geomagn. Geoelectr.*, **42**, 1019-1036.

HAINES, G.V. (1990): Regional magnetic field modelling: a review, *J. Geomagn. Geoelectr.*, **42**, 1001-1018.

MALIN, S.R.C., D.R. BARRACLOUGH and B.M. HODDER (1982): A compact algorithm for the formation and solution of normal equations, *Comput. Geosci.*, **8** (3-4), 355-388.

MAYHEW, M.A. (1979): Inversion of satellite magnetic anomaly data, *J. Geophys.*, **45**, 119-128.

MEYER, J., J.H. HUFEN, M. SIEBERT and A. HAHN (1983): Investigation of the internal geomagnetic field by means of a global model of the Earth's crust, *J. Geophys.*, **52**, 71-84.

NAKAGAWA, I. and T. YUKUTAKE (1985): Rectangular harmonic analyses of geomagnetic anomalies derived from MAGSAT data over the area of the Japanese islands, *J. Geomagn. Geoelectr.*, **37**, 957-977.

NOLTE, H.J. and A. HAHN (1992): A model of the distribution of crustal magnetization in Central Europe compatible with the field of magnetic anomalies deduced from MAGSAT results, *Geophys. J. Int.*, **111**, 483-496.

O'BRIEN, M.S. and R.L. PARKER (1994): Regularized geomagnetic field modelling using monopoles, *Geophys. J. Int.*, **118**, 566-578.

PURUCKER, M.E. (1990): The computation of vector magnetic anomalies: a comparison of techniques and errors, *Phys. Earth Planet. Inter.*, **62**, 231-245.

TAYLOR, P.T. and D. RAVAT (1995): An interpretation of the MAGSAT anomalies of Central Europe, *J. Appl. Geophys.*, **34**, 83-81.

(received November 21, 1997;
accepted March 13, 1998)